Knudsen Diffusivity and Permeability of PEMFC Microporous Coated Gas Diffusion Layers for Different Polytetrafluoroethylene Loadings

Nicholas B. Carrigy[1], Lalit M. Pant[1,2], Sushanta Mitra[2], and Marc Secanell[1]

[1] *Energy Systems Design Laboratory, Department of Mechanical Engineering, University of Alberta, Edmonton, Alberta, Canada T6G 2G8*

[2] *Micro and Nano-Scale Transport Laboratory, Department of Mechanical Engineering, University of Alberta, Edmonton, Alberta, Canada T6G 2G8*

Abstract

The Knudsen diffusivity and viscous permeability of proton exchange membrane fuel cell microporous coated gas diffusion layers are obtained experimentally for different polytetrafluoroethylene loadings. Pressure drop across the microporous coated gas diffusion layers is measured at varying flow rates and using different gases. A semi-empirical expression proposed by Knudsen is used to analyze the experimental results and is shown to accurately predict gas transport in microporous coated gas diffusion layers. The Knudsen diffusivity of the microporous coated gas diffusion layers is shown to decrease with increased PTFE loading. The compressible form of Darcy's law is shown to overestimate the viscous permeability of microporous coated gas diffusion layers because it cannot account for gas slip at the pore walls.

1.0 Introduction

Designing a fuel cell that can operate at high current densities requires modifying the membrane electrode assembly in order to enhance mass transport. Therefore, accurate predictions of the relationships between fuel cell morphology and the coupled physical processes occurring inside the cell are required. Mass transport losses at the cathode due to an inadequate supply of oxygen to the catalyst layer prevent efficient operation of the fuel cell at high current densities. The supply of oxygen to the cathode catalyst layer, and the rejection of water to the flow channels, can be quantified in part by the permeability and Knudsen diffusivity of the microporous layer (MPL) coated gas diffusion layer (GDL). A recent study suggested that Knudsen diffusivity may account for up to 80% of the effective diffusivity in the MPL [1].

The GDL is often treated with polytetrafluoroethylene (PTFE) to increase its hydrophobicity. The PTFE can be applied as an aqueous solution using spray, brush, flow, or immersion techniques [2]. PTFE is usually applied via the immersion technique which allows for the best control of PTFE loading; however, a key drawback of the immersion technique is a lack of control of the PTFE distribution in the through-plane direction [2]. The PTFE tends to accumulate near the surface of the GDL and at the intersection between fibers, thus reducing the porosity and shrinking the pore size distribution. MPLs are typically made using carbon graphite nanoparticles, PTFE, and a pore forming salt [3].

The GDL and MPL are often treated as separate entities and the mass transport properties of each entity are determined independently. Fishman and Bazylak [3,4] recently used micro-computed tomography (μCT) reconstruction to study the through-plane porosity distribution of SGL GDL and MPL samples and found significant intrusion of the MPL into the GDL. Martinez-Rodriguez et al. [5] found using scanning electron microscope (SEM) imaging that the GDL merged with the MPL and that no clear separating boundary could be defined. These results would imply that treating the GDL and MPL as separate entities with discrete thicknesses and distinct mass transport properties may not accurately capture the behavior of the combined gas diffusion - microporous layer (GDL/MPL). This study provides SEM and μCT images of GDL/MPLs which show non-uniform MPL intrusion into the GDL; therefore, distinct GDL and MPL mass transport properties are not quantified. Rather, combined GDL/MPL mass transport properties are determined.

The permeability of GDLs without MPLs has been determined experimentally by many authors. Williams et al. [6] determined the gas permeability of carbon cloth and carbon paper GDLs. Prasanna et al. [7] measured the gas permeability of A-T2 carbon paper for various PTFE loadings. Park et al. [8] determined the air permeability of Toray carbon paper for various PTFE loadings. Gostick et al. [9] determined the absolute gas permeability of GDLs in three perpendicular directions. This included measuring the effect of compression on the in-plane permeability values [9]. Feser et al. [10] determined the in-plane permeability of gas diffusion layers for various compression levels. Lobato et al. [11] determined the air permeability of Toray TGP 120 with various PTFE loadings. Hussaini and Wang [12] determined the absolute and relative permeability of water and air in the through-plane and in-plane directions for untreated Toray carbon paper and E-Tek carbon cloth. Ismail et al. [13] determined the effect of PTFE treatment on the through-plane permeability of SGL and Ballard GDLs. Tamayol and Bahrami [14] measured the in-plane permeability of GDLs and Tamayol et al. [15] measured the effect of compression and PTFE loading on the through-plane gas permeability of Toray 120.

The permeability of MPLs has been given less attention in the literature. Gurau et al. [16] determined the through-plane and in-plane permeability of carbon cloth GDLs with MPLs for 30 % and 70 % PTFE loadings using the Darcy-Forchheimer equation. Ismail et al. determined the effect of PTFE treatment and MPL coating on the in-plane permeability of SGL GDLs [17] and the through-plane permeability of SGL and Ballard MPL coated GDLs [18] using the compressible form of Darcy's law. Pant et al. [19] quantified the viscous permeability of an SGL 34 BC and proposed the use of the Binary Friction Model (BFM) for obtaining more accurate permeability estimates.

Knudsen diffusivity has gained interest in the recent literature. Recently, Pant et al. [19] estimated the Knudsen diffusivity of the MPL and GDL of an SGL 34 BC separately using the BFM. Pant et al. [19] found that the conventional Darcy-Forchheimer model is not capable of estimating gas independent permeability, as it does not account for Knudsen diffusion in the MPL. Chan et al. [1] estimated the effective diffusivity of GDLs and MPLs using a Loschmidt cell and concluded that Knudsen diffusivity may account for 80 % of the effective diffusivity.

In this article, Knudsen diffusivity is determined for GDL/MPLs with different PTFE loadings by means of a recently developed gas permeability apparatus in combination with a semi-empirical expression developed by Knudsen. This is the first study to quantify the effect of GDL PTFE loading on the Knudsen diffusivity and viscous permeability of GDL/MPL assemblies. The degree of viscous permeability overestimation due to application of the compressible form of Darcy's law to GDL/MPL assemblies is quantified for different PTFE loadings.

Section 2 presents the experimental setup, an experimental error analysis, and SEM and μCT images showing PTFE and MPL distributions in the GDL. Section 3 provides a brief discussion of the Knudsen number and the mathematical mass transport models used: the compressible form of Darcy's law and Knudsen's expression. Section 4 presents the viscous permeability of GDLs and GDL/MPLs with different PTFE loadings in the GDL calculated using the compressible form of Darcy's law, the Knudsen diffusivity and viscous permeability of GDL/MPLs with different PTFE loadings in the GDL calculated using Knudsen's expression, and experimental validation of the predicting capabilities of Knudsen's expression for different gas types.

2.0 Materials and Methods

2.1 Description of experimental apparatus

Figure 1 shows a schematic of the modified diffusion bridge used to determine the pressure drop through the porous layers at varying gas flow rates. The modified diffusion bridge used in this study was originally developed by Pant et al. [19] and has been automated using LabWindows/CVI for more convenient use.

Gas (Praxair, all with purity 99.993 % or higher) from a compressed cylinder flowed through a mass flow controller (Cole Parmer, model: RK-32907-69 for GDL testing; Cole Parmer, model: RK-32907-57 for GDL/MPL testing) which controlled the flow rate and therefore velocity through the porous layers. A pressure transducer (Omegadyne Inc., model: MMDDB001BIV10H2A0T1A2) measured the static pressure difference upstream of the porous materials so that dynamic pressure caused by the gas velocity through the porous materials did not affect the reading. LabWindows/CVI was used to read the pressure difference passed from the pressure transducer through the data acquisition card (National Instruments USB 6221) to the computer. The program incremented the mass flow controller in even steps from 0 to 0.050 slpm during GDL tests and from 0 to 10 sccm during GDL/MPL tests. The program calculated the pressure drop per unit thickness and velocity through the porous materials every 5 seconds and saved all data to a text file. Readings were taken at every mass flow rate setpoint for 10 minutes to ensure steady state was reached; steady state was verified from the logged data.

To prepare the porous layers for testing they were cut into 1.5 cm by 2.5 cm pieces and 3 layers were stacked. For GDL/MPLs, 2 layers were stacked with the MPL sides facing each other. The stacked layers were laminated (HeatSeal H220 Laminator) in 3 mil lamination sheet which had a 2.1 ± 0.1 mm aperture hole punched into it, as measured by a surface profilometer (AMBIOS XP-300). The aperture hole provided a path for the gas to transport through the porous layers. The laminated sheet containing the porous layers was placed between silicone sealing gaskets which prevented gas leakage and ensured no additional compression due to assembly via bolting between 2 acrylic blocks containing flow channels of 3mm x 3 mm cross section.

2.2 Experimental error analysis

GDLs without a microporous coating were tested for the purpose of validating the experimental setup and therefore only one run was performed with each GDL. The exception was the SGL 34 BA, for which repeatability of the apparatus for the same sample under the same conditions was ± 2 %, the variation between samples cut from the same sheet was ± 7 %, and the variation between samples cut from different sheets was ± 18 %.

Determining the Knudsen diffusivity and viscous permeability of the GDL/MPL samples was the focus of this study and therefore three tests were performed at each PTFE loading. The three tests were performed using different samples cut from the same sheet. Results are reported as mean ± standard deviation where applicable.

Parametric studies regarding placement of the pressure transducer, the number of layers stacked, the aperture hole size, and the orientation of the cell were performed. The number of GDLs stacked to produce repeatable viscous permeability results was 3 to 4 layers. Similarly, Martinez-Rodriguez et al. [5] found that 4 to 5 layers of GDLs had to be stacked to produce consistent results for the MacMullin number (ratio of bulk-to-effective diffusivity). Stacking allows a more representative number of fibers to be present in the through-plane direction, although it can lead to slight fiber overlap. The stacking method slightly compresses the samples and therefore it is likely that a cell which does not compress the layers would produce viscous permeability results less than this study. However, the results from this study are in agreement with those reported in the literature. Varying the cross-sectional area in the through-plane direction produced less error than the variation between GDLs from different batches. The orientation of the cell did not affect the results.

2.3 Materials

Toray TGP 090 GDLs with 0, 5, 10, 20, and 40 % PTFE loadings were provided by the Automotive Fuel Cell Cooperation (AFCC) and used for experimental validation, as was an SGL 34 BA. Four GDL/MPLs with 5, 10, 20, and 40 % PTFE loadings in the GDL and the same MPL ink formulation and fabrication method also provided by AFCC were tested, as well as a commercial SGL 34 BC. The PTFE loading in the MPL was the same for all Toray samples but was not specified.

The thickness of the layers was measured individually prior to stacking, as stacked, and after lamination with a micrometer (Mitutoyo, Japan) at a load setting of 0.5 N. The compressed thickness per layer and overall compression of the GDL samples is given in Table 1. The thickness of the Toray GDL was similar to the corresponding Toray GDL/MPL for every PTFE loading indicating MPL intrusion into the GDL.

A qualitative characterization of the GDLs and GDL/MPLs used in this study was produced using SEM and μCT imaging. The objective of the imaging was to examine: (a) the PTFE distribution within the GDL; and, (b) the MPL intrusion into the GDL.

Top views of the GDLs obtained via SEM imaging (JEOL 6301F, Field Emission SEM) were compared to examine the change in pore size and PTFE distribution for different PTFE loadings, and also to obtain fiber diameter estimates.

Figures 2 (a) to (c) show a noticeable decrease in pore size between Toray GDLs with 0, 5, and 10 % PTFE loadings, respectively. It is reasonable to infer from Figures 2 (b) and (c) that the PTFE tends to accumulate at the intersection between fibers thus reducing the pore size. At 5 % PTFE loading, the PTFE deposits in the small pores at the intersections of the fibers but leaves the large pores still available for mass transport. The gas flow in these smaller pores which connect the larger pores is likely driven significantly by Knudsen diffusion. The SGL 34 BC PTFE shown in Figure 2 (d) appeared more granular than the Toray PTFE. The Toray fiber diameter was estimated to be 9.0 ± 0.2 μm and the SGL 34 BC fiber diameter to be 7.5 ± 0.1 μm using images not shown.

To verify intrusion of the MPL into the GDL, cross-sectional SEM images were obtained for each GDL/MPL. The samples were prepared by freeze fracturing using tweezers after immersion in liquid nitrogen. Sample preparation via freeze fracturing showed the internal structure more clearly than did cutting the sample with a knife.

Figures 3 (a) and (b) show side view images of Toray GDL/MPLs with 10 and 20 % PTFE loading in the GDL, respectively. It can be seen that the distinction between the GDL and MPL is not clear for either Toray sample. Using side view images not shown the SGL 34 BC MPL thickness was estimated at two different locations along the same sample. The estimates at the two different locations were 58 and 72 µm indicating non-uniform MPL intrusion into the GDL.

To examine preferential pathways for mass transport in GDL/MPLs, SEM images were taken of the MPL side. Figure 4 (a) shows GDL fibers present in the MPL side of the Toray GDL/MPL. Fibers were found in multiple samples. Separating the GDL and MPL properties would lead to error since the presence of GDL fibers is shown to affect the MPL structure. In the MPL of the Toray sample, pores on the order of 10 µm are clearly visible.

Figure 4 (b) shows that cracks are also present in the SGL 34 BC sample. The cracks do not appear to intrude completely through the MPL. The cracks are around 50 µm in width but varied at different locations along the MPL. These cracks provide a preferential path for gas to transport through the layer before reaching connected pores further into the depth of the MPL, thus decreasing the distance through which the gas transports in the small MPL pore structure.

To further examine MPL intrusion into the GDL, high resolution x-ray µCT images of an SGL 34 BC sample were obtained (SkyScan 1172, Belgium) at 1.79 µm per voxel. The program NRecon was used to clean up the images. DataViewer was then used to create a 3D reconstruction of the sample. Images are shown in Figures 5 (a) to (c) for local depths as measured from the GDL side of 83, 167, 247, and 283 µm into the sample, respectively. The onset of black space on the right hand side of Figures 5 (a) to (d) indicates the end of the sample.

Figure 5 (a) shows the structure near the SGL 34 BC GDL surface, where darker areas between GDL fibers represent void space. The PTFE tends to accumulate non-uniformly at the surface of the GDL, causing fiber cluster formation. This fiber cluster formation results in non-uniform mass transport at the GDL surface. Flow through these clusters is likely affected by slip due to the smaller pore sizes.

Figure 5 (b) shows MPL intrusion into the GDL at some locations, but not throughout the sample. This evidence of non-uniform MPL intrusion into the GDL indicates that, for the samples under study, the MPL and GDL should not be treated as separate entities with discrete thicknesses. The GDL alters the MPL structure and vice versa at this depth into the sample.

Figure 5 (c) shows the internal structure of the MPL which contains cracks and pores. Significantly less PTFE is present at this depth than near the GDL surface indicating a non-uniform PTFE distribution within the GDL.

Figure 5 (d) is a cross-sectional image into the width of the sample showing MPL intrusion and large pores in the MPL. Since Figure 5 (d) was taken at a (non-physical) slice into the width of the sample, the MPL intrusion could not have been caused by sample preparation or handling.

It is desirable to separate the GDL and MPL properties to quantify the effect of pore structure on mass transport properties; however, for the GDL/MPLs in this study, the presence of GDL fibers in the MPL indicated that only the combined GDL/MPL properties can be accurately determined. Separating the GDL and MPL properties based on discrete thickness values could lead to misleading results for the examined samples. Therefore, all analysis in the following sections was performed using combined GDL/MPL properties.

3.0 Theory

3.1 Knudsen number

For flow in porous media the Knudsen number can be given by [20]:

$$Kn = \frac{\lambda}{d_p} \tag{1}$$

where λ is the mean free path length of the permeating gas and d_p is the mean pore diameter. Based on the Knudsen number, different flow regimes can be defined. In the continuum regime, $Kn < 0.001$, the Navier-Stokes equations can be applied with a no-slip boundary condition [21]. Darcy's law is only applicable in the continuum regime and has been derived based on the Stokes equation and a no-slip boundary condition [22]. A slip boundary condition is required between continuum and free molecular flow, i.e. $0.001 \leq Kn \leq 10$ [21]. Due to small mean pore diameters flow in GDL/MPLs falls within this range [19].

3.2 Compressible form of Darcy's law

Assuming one dimensional gas flow the differential form of Darcy's law is given by [23]:

$$N = -\frac{B_v}{\eta}\frac{p}{R_g T}\frac{dp}{dx} \tag{2}$$

where N is the molar flux, B_v is the viscous permeability, η is the gas viscosity, p is the pressure, R_g is the gas constant, T is the temperature, and x is the spatial coordinate taken as positive in the direction of flow.

At steady state, N is constant due to mass conservation. For simplicity, isothermal conditions are assumed and the viscosity is taken as a constant. Equation (2) is integrated from the inlet of the porous media, x_1, to the outlet of the porous media, x_2, as follows:

$$\frac{NR_gT\eta}{B_v}\int_{x_1}^{x_2} dx = \int_{p_1}^{p_2} -p dp \tag{3}$$

$$\frac{NR_gT\eta L}{B_v} = \frac{p_1^2 - p_2^2}{2} \tag{4}$$

where $L = x_2 - x_1$ is the thickness of the porous layer in the direction of flow. The inlet pressure $p_1 = p_2 + \Delta p$ where p_2 is taken as the ambient pressure and Δp is the pressure drop measured by the pressure transducer.

The molar flux is given by:

$$N = \frac{pv}{R_gT} \tag{5}$$

Isothermal conditions are assumed and the molar flux is constant at steady state. Therefore, the product of velocity and pressure is constant at any given distance x into the porous media. Hence:

$$pv = p_1v_1 \tag{6}$$

The inlet velocity, v_1, is calculated from the inlet flow rate, Q_1, and the aperture diameter in the lamination sheet, d_{ap}, according to:

$$v_1 = \frac{4Q_1}{\pi d_{ap}^2} \tag{7}$$

The inlet flow rate is given by the mass flow controller, as a negligible pressure drop occurs in the gas prior to entering the porous media.

Equation (6) is substituted into equation (5), which is further substituted into equation (4), and after simple rearrangement and cancellation the compressible form of Darcy`s law is obtained:

$$v_1 = \frac{B_v}{2\eta L}\left(\frac{p_1^2 - p_2^2}{p_1}\right) \tag{8}$$

Equation (8) is solved in MATLAB using a least-squares curve fit to the experimental data and the permeability value is obtained.

3.3 Knudsen's expression

Knudsen proposed a semi-empirical expression to predict gas flow in all regimes based on his experimental measurements of gas flow in capillaries, as explained in Cunningham and Williams [23]. At sufficiently high pressures Knudsen's expression for a capillary can be simplified to [23]:

$$N = -\left(\frac{R^2}{8\eta}\frac{p_1 + p_2}{2} + D^k\frac{c_1^k}{c_2^k}\right)\frac{1}{R_g T}\frac{p_2 - p_1}{x_2 - x_1} \tag{9}$$

where *R* is the radius of the capillary, a^K, b^K, c_1^k, and c_2^k are constants that depend on the gas and capillary, and D^k is the Knudsen diffusivity.

Equation (9) is similar in form to the Klinkenberg equation which relates the intrinsic (no-slip) liquid permeability to the gas permeability through a gas-dependent wall-slip [24]. The differential form of equation (9) is also similar in form to the Maxwell slip equation [25]. Kerkhof [25] used this latter similarity in his BFM to suggest that for engineering purposes:

$$\frac{c_1^k}{c_2^k} \approx 0.89 \tag{10}$$

The Knudsen diffusivity in a capillary is given by [23]:

$$D^k = d\frac{1}{3}\sqrt{\frac{8R_g T}{\pi M}} \tag{11}$$

where *d* is the diameter of the capillary and *M* is the molar mass of the gas.

To apply Knudsen's expression to porous media, the following substitutions are made [19]:

$$\frac{R^2}{8} => B_v \tag{12}$$

$$0.89D^k => D^{k,eff} \tag{13}$$

The relationship between the viscous permeability of a capillary and the viscous permeability of a porous media is given by the intrinsic properties of the porous media, such as the porosity and tortuosity, and can therefore be determined experimentally. Similarly, the effective Knudsen diffusivity is related to the Knudsen diffusivity in a capillary by the intrinsic porous material geometry. Therefore, in this model the effective Knudsen diffusivity is only a function of the molar mass of the gas and the porous material geometry (assuming isothermal conditions) and can be determined experimentally.

The GDL/MPLs in this study were shown in Section 2.3 to have complex pore geometries. The proposed model is based on effective transport properties and therefore it estimates an effective pore diameter only. The proposed effective pore diameter is a function not only of the mean pore diameter of the porous media but also of its porosity and tortuosity. Detailed information regarding the impact of the pore geometry on gas transport cannot be obtained from the proposed effective diameter. To obtain such information a detailed three dimensional reconstruction of the MPL together with either a continuum based model with slip boundary conditions or a non-continuum based gas transport model would be required.

In this model, the effective Knudsen diffusivity is obtained for a combined GDL/MPL assembly. Ideally, the effective Knudsen diffusivity of the GDL and MPL would be determined separately to obtain further information regarding the effective pore diameter of each layer. However, for the samples under study, MPL intrusion into the GDL was found to alter the structure of the MPL (Figure 4 (a)), thus preventing separate analysis of the GDL and MPL based on discrete thickness values. In this study the MPL ink formulation was the same for all Toray samples; however, this study later shows (Section 4.3) that the effective Knudsen diffusivity changes substantially with GDL treatment which further highlights the impact of the GDL structure on the MPL intrusion and morphology. Hence, a direct relation between the mean pore diameter and effective pore diameter is not specified for the GDL/MPLs due to the complex pore structure.

Applying the substitutions in equations (11), (12), and (13) to equation (9) gives:

$$N = -\left(\frac{B_v}{\eta}\frac{p_1 + p_2}{2} + D^{k,eff}\right)\frac{1}{R_g T}\frac{p_2 - p_1}{x_2 - x_1} \tag{14}$$

Equation (14) can also be obtained by integrating the Kerkhof's BFM across the porous media [26]. The molar flux, N, is constant at steady state and therefore equation (6) is substituted into equation (5), which is further substituted into equation (14). After cancellation of the gas constant and temperature:

$$p_1 v_1 = -\left(\frac{B_v}{\eta}\frac{p_1 + p_2}{2} + D^{k,eff}\right)\frac{p_2 - p_1}{x_2 - x_1} \tag{15}$$

The right hand side of equation (15) is separated into two terms and isolated for v_1 noting that $L = x_2 - x_1$ to obtain:

$$v_1 = \frac{B_v}{2\eta L}\left(\frac{p_1^2 - p_2^2}{p_1}\right) + \frac{D^{k,eff}}{L}\left(\frac{p_1 - p_2}{p_1}\right) \tag{16}$$

The effective Knudsen diffusivity is a function of the gas and pore geometry. In order to obtain an intrinsic property of the porous material, an effective pore diameter, d_p^{eff}, is defined such that [19]:

$$D^{k,eff} = 0.89\, d_p^{eff}\,\frac{1}{3}\sqrt{\frac{8R_g T}{\pi M}} \tag{17}$$

Substituting equation (17) into equation (16) gives:

$$v_1 = \frac{B_v}{2\eta L}\left(\frac{p_1^2 - p_2^2}{p_1}\right) + 0.89\frac{d_p^{eff}}{3L}\sqrt{\frac{8R_gT}{\pi M}}\left(\frac{p_1 - p_2}{p_1}\right) \tag{18}$$

In order to solve equation (18) for B_v and d_p^{eff}, numerical fitting via the method of non-linear least squares can be performed. Pressure drop versus velocity data from one test using nitrogen gas and one separate test using helium gas are fitted using a non-linear least square optimization in MATLAB to decrease the sensitivity of the model to fitting error. The non-linear least square optimization is given by:

$$e = \sum_{i=1}^{n}\left[v_{1,exp} - v_{1,num}\left(B_v\,, d_p^{eff}\right)\right]^2 \tag{19}$$

where e represents the residual, $v_{1,exp}$ is the experimental velocity obtained from equation (7), and $v_{1,num}$ is the numerical estimate of the velocity obtained from equation (18) based on guesses of B_v and d_p^{eff}. The values of B_v and d_p^{eff} which result in minimum residual represent the gas-independent solution for the viscous permeability and effective pore diameter of the porous layers.

4.0 Results and Discussion

4.1 Compressible form of Darcy's law applied to GDLs

The compressible form of Darcy's law given in equation (8) was first applied to GDLs to validate the experimental apparatus and to determine if variations in viscous permeability are obtained when different gas types are used. Variations in viscous permeability between tests with different gas types would indicate that gas slip is present. In addition, the effect of PTFE loading on the viscous permeability of the GDL was studied.

For GDLs and nitrogen gas, the Knudsen number is near the continuum regime limit of 0.001 and therefore the compressible form of Darcy's law should fairly accurately describe the flow [19]. Pressure drop versus velocity results for the Toray GDLs with different PTFE loadings obtained using nitrogen as the working gas are given in Figure 6. As shown, the pressure drop across the GDLs increase with PTFE loading as expected due to smaller pores, as also observed in Section 2.3.

The viscous permeability obtained using the compressible form of Darcy's law with nitrogen as the working gas is compared to the literature values in Table 2. Gostick et al. [9] measured the through-plane permeability of SGL 34 BA using the compressible form of Darcy's law. Hussaini and Wang [12] measured the through-plane permeability of SGL 34 BA using the incompressible form of Darcy's law. The difference between the SGL 34 BA viscous permeability obtained by Gostick et al. [9] and in this study is within the experimentally determined variation between batches of ± 18 %. The results for untreated Toray 090 are within the literature values obtained by Gostick et al. [9] and Hussaini and Wang [12]. The experimental apparatus was considered validated.

In the same porous layer, gases with long mean free path lengths such as helium (~ 195 nm at 25 °C and 100 kPa) have higher Knudsen numbers than gases with low mean free path lengths such as nitrogen (~ 65.9 nm at 25 °C and 100 kPa). Slip flux contributes to mass transport to a greater extent relative to pure viscous flux at higher Knudsen numbers and therefore the effect of slip is expected to be more pronounced for tests with helium than for tests with nitrogen. To show the effect of slip in GDLs, the viscous permeability results for the GDLs with different PTFE loadings are compared in Table 3 for separate tests using nitrogen and helium as calculated using the compressible form of Darcy's law, given by equation (8). The viscosity of nitrogen and helium were taken as 1.82×10^{-5} and 2.02×10^{-5} Pa s, respectively.

The pure viscous permeability of a porous layer is an intrinsic property and should be independent of the gas type used. If no gas slip occurs the ratio of viscous permeability obtained using the compressible form of Darcy's law from tests with different gas types should equal one. However, Table 3 indicates a higher viscous permeability estimate for helium, the gas with a higher Knudsen number in the GDL. Therefore, the compressible form of Darcy's law produces gas-dependent viscous permeability estimates due to gas slip. For GDLs, this effect is not too pronounced as relatively low intermediate regime Knudsen numbers apply.

The ratio of nitrogen to helium viscous permeability calculated using the compressible form of Darcy's law decreased with increasing PTFE loading. This is due to smaller pore diameters in GDLs with higher PTFE loading (Section 2.3), which increases the relative contribution of gas slip to mass transport. With increased gas slip the compressible form of Darcy's law less accurately describes the flow, as it requires a no-slip boundary condition.

4.2 Compressible form of Darcy's law applied to GDL/MPLs

The viscous permeability was obtained for GDL/MPLs in a similar manner to GDLs to show that a gas-independent viscous permeability cannot be obtained for the GDL/MPLs using the compressible form of Darcy's law as it cannot account for gas slip at the pore walls. Typical pressure drop versus velocity profiles for the GDL/MPLs with nitrogen gas are given in Figure 7. The pressure drop across the GDL/MPL was found to be significantly affected by the PTFE loading in the GDL. This would imply that for the samples under study the mass transport properties of the GDL/MPL are not governed by the MPL alone.

The viscous permeability of the GDL/MPLs for nitrogen and helium tests are given and compared in Table 4. The uncertainty in the viscous permeability may be due to manufacturing uncertainties, or the holes and cracks in the MPL which provide preferential paths for mass transport. These holes and cracks are likely incurred during manufacturing and provide preferential pathways for mass transport.

The viscous permeability of the GDL/MPLs decreased significantly for 10, 20, and 40 % PTFE loading in the GDL indicating a strong dependence of GDL/MPL properties on the GDL PTFE loading. The viscous permeability results obtained between the Toray 5 and 10 % PTFE loading are within one standard deviation of each other but increased slightly for both gas types.

Recall that the pure viscous permeability of a porous layer is an intrinsic property and therefore should be independent of the gas type used. If no gas slip occurs the ratio of viscous permeability obtained using the compressible form of Darcy's law from tests with nitrogen and helium should equal one. The ratio of helium to nitrogen GDL/MPL viscous permeability calculated using the compressible form of Darcy's law was higher than one, as the additional flux due to gas slip was attributed to pure viscous transport. These results indicate that the compressible form of Darcy's law cannot be used to model gas transport in the GDL/MPLs and further indicates that gas slip should be taken into account for accurate determination of the intrinsic viscous permeability of GDL/MPLs.

4.3 Knudsen's expression applied to determine the Knudsen diffusivity and viscous permeability of GDL/MPLs

The Knudsen diffusivity and viscous permeability of the GDL/MPLs were obtained using equation (18) and equation (19) as discussed in Section 3.3. The results are given in Table 5 for different GDL PTFE loadings. The effective Knudsen diffusivity for oxygen, nitrogen, and hydrogen gas was calculated from the effective pore diameter using equation (17) and is also given in Table 5.

The effective pore diameters obtained using Knudsen's expression were 2.10 ± 0.02, 1.8 ± 0.2, 0.9 ± 0.1, and 0.38 ± 0.08 μm for Toray 090 with 5, 10, 20, and 40 % PTFE loadings in the GDL, respectively. This indicates that the PTFE loading in the GDL significantly affects the effective pore diameter of the GDL/MPL, as the same MPL coating was used in all Toray samples. Hence, the MPL properties did not solely dominate for the Toray GDL/MPLs under study. The effective pore diameter of the SGL 34 BC obtained using Knudsen's expression was 2.07 ± 0.01 μm.

The Knudsen diffusivity was found to decrease for increased PTFE loading in the GDL. This does not imply that the Knudsen diffusivity, and hence gas slip, becomes less important with increasing PTFE loading since the Knudsen diffusivity of the GDL/MPL tended to decrease at a lesser rate than the viscous permeability. Knudsen diffusivity scales with the pore diameter whereas viscous permeability scales with the square of the pore diameter. Therefore, slip contributes to mass transport to a greater extent in GDL/MPLs with more PTFE loading in the GDL.

The viscous permeability of the Toray 090 GDL/MPLs obtained using Knudsen's expression are 3.3 ± 0.3, 3.6 ± 0.8, 1.1 ± 0.2, and 0.4 ± 0.1 x 10^{-13} m^2 for 5, 10, 20, and 40 % PTFE loadings, respectively, showing a decreasing trend with increased PTFE loading in the GDL. The viscous permeability obtained using Knudsen's expression is independent of the gas, as results from tests with two different gas types are fitted simultaneously. The viscous permeability of the SGL 34 BC sample obtained using Knudsen's expression was 6.0 ± 0.2 x 10^{-13} m^2.

In Table 6, the gas-dependent viscous permeability obtained using the compressible form of Darcy's law is compared to the gas-independent viscous permeability obtained using Knudsen's expression. The quotient of the Knudsen expression viscous permeability estimate and compressible form of Darcy's law viscous permeability estimate for a given PTFE loading was calculated and then averaged, as opposed to dividing the average viscous permeability values given in Table 4 and Table 5. The viscous permeability obtained using the compressible form of Darcy's law overestimated the viscous permeability as compared to Knudsen's expression by a factor of 1.096 ± 0.003 to 1.29 ± 0.05 for nitrogen and a factor of 1.29 ± 0.02 to 1.9 ± 0.1 for helium. Recall that the overestimation is higher for helium due to a longer mean free path length and therefore relatively higher contribution of gas slip to mass transport.

The viscous permeability overestimation due to application of the compressible form of Darcy's law tended to increase with PTFE loading for both gas types due to smaller pore sizes (Section 2.3). Hence, gas slip should be taken into account to determine the intrinsic viscous permeability of GDL/MPLs.

4.4 Validation of Knudsen's expression using argon and oxygen gas

Predictions of the pressure drop versus velocity profile for GDL/MPLs can be estimated for other gas types not tested in the previous sections using the effective pore diameter and viscous permeability obtained using Knudsen's expression. Predicted values are obtained by changing only the gas viscosity (2.29×10^{-5} and 2.05×10^{-5} Pa s for argon and oxygen, respectively) and the molar mass in equation (18). The effective pore diameter and viscous permeability from analysis of a single Toray 090 GDL/MPL with 5 % PTFE loading in the GDL were 2.1 µm and 3.3×10^{-13} m^2. Using the compressible form of Darcy's law the viscous permeability of the same sample was found to be 4.96×10^{-13} m^2 using helium gas.

Figure 8 compares pressure drop versus velocity profile predictions for argon and oxygen gas transport through the Toray 5 % PTFE GDL/MPL sample determined using the effective properties to experimentally obtained results with argon and oxygen as the working gas. Knudsen's expression predicts pressure drop versus velocity profiles for argon and oxygen gas which are in agreement with this experiment. The compressible form of Darcy's law predicts pressure drop versus velocity profiles which are inconsistent with this experiment. Therefore, Knudsen's expression provided a more accurate prediction of mass transport in the Toray GDL/MPL sample than the compressible form of Darcy's law.

5.0 Conclusion

Knudsen's expression was used to determine the Knudsen diffusivity and viscous permeability of an SGL 34 BC and Toray GDL/MPLs with the same MPL ink formulation and different PTFE loadings in the GDL. The Knudsen diffusivity of the Toray GDL/MPLs was found to decrease with increased PTFE loading. Knudsen's expression was capable of accurately predicting pressure drop versus velocity profiles whereas the compressible form of Darcy's law was not. A gas-dependent viscous permeability was observed when the compressible form of Darcy's law was applied to GDLs and GDL/MPLs. The compressible form of Darcy's law cannot account for gas slip at the pore walls and therefore overestimated the viscous permeability significantly as compared to Knudsen's expression. Knudsen's expression was shown to provide an accurate method for analyzing and predicting gas transport in GDL/MPLs.

Acknowledgements

Financial assistance from the Natural Sciences and Engineering Research Council of Canada and the Automotive Fuel Cell Cooperation is gratefully acknowledged. The authors would like to thank Mr. Josh Seens of the SEM Laboratory at the University of Alberta for taking SEM images and Dr. Phil Salmon of SkyScan for instruction on µCT reconstruction.

References

[1] C. Chan, N. Zamel, X. Li, and J. Shen, *Electrochim. Acta,* **65**, 13 (2012).

[2] A. Rofaiel, J.S. Ellis, P.R. Challa, and A. Bazylak, 2012, *J. Power Sources*, **201**, 219 (2012).

[3] Z. Fishman and A. Bazylak, *J. Electrochem. Soc.*, **158** (8), B846 (2011).

[4] Z. Fishman and A. Bazylak, *J. Electrochem. Soc.*, **158** (8), B841 (2011).

[5] M.J. Martinez-Rodriguez, T. Cui, S. Shimpalee, S. Seraphin, B. Duong, and J.W. Van Zee, *J. Power Sources*, **207**, 91 (2012).

[6] M.V. Williams, E. Begg, L. Bonville, H.R. Kunz, and J.M. Fenton, *J. Electrochem. Soc*., **151**, A1173 (2004).

[7] M. Prasanna, H.Y. Ha, E.A. Cho, S.-A. Hong, and I.-H. Oh, *J. Power Sources*, **131**, 147 (2004).

[8] G.-G. Park, Y.-J. Sohn, T.-H. Yang, Y.-G. Yoon, W.-Y. Lee, and C.-S. Kim, *J. Power Sources*, **131**, 182 (2004).

[9] J.T. Gostick, M.W. Fowler, M.D. Pritzker, M.A. Ioannidis, and L.M. Behra, *J. Power Sources*, **162**, 228 (2006).

[10] J.P. Feser, A.K. Prasad, and S.G. Advani, *J. Power Sources*, **162**, 1226 (2006).

[11] J. Lobato, P. Cañizares, M.A. Rodrigo, C. Ruiz-López, and J.J. Linares, *J. Appl. Electrochem.*, **38**, 793 (2008).

[12] I.S. Hussaini and C.Y. Wang, *J. Power Sources*, **195,** 3830 (2010).

[13] M.S. Ismail, T. Damjanovic, K. Hughes, D.B. Ingham, L. Ma, L., M. Pourkashanian, and M. Rosli, *J. Fuel Cell Sci. Technol.*, **7**, 051016-1 (2010).

[14] A. Tamayol and M. Bahrami, *J. Power Sources*, **196**, 3559 (2011).

[15] A. Tamayol, F. McGregor, and M. Bahrami, *J. Power Sources*, **204**, 94 (2012).

[16] V. Gurau, M.J. Bluemle, E.S. De Castro, Y.-M. Tsou, T.A. Zawodzinski Jr., and J. Adin Mann Jr., *J. Power Sources*, **165**, 793 (2007).

[17] M.S. Ismail, T. Damjanovic, D.B. Ingham, L. Ma, and M. Pourkashanian, *J. Power Sources*, **195**, 6619 (2010).

[18] M.S. Ismail, D. Borman, T. Damjanovic, D.B. Ingham, and M. Pourkashanian, *Int. J. Hydrogen Energy*, **36**, I0392 (2011).

[19] L.M. Pant, S.K. Mitra, and M. Secanell, *J. Power Sources*, **206**, 153 (2012).

[20] G.L. Vignoles, *J. Phys. Col.*, **5**, C5-159 (1995).

[21] R.K. Agarwal, K.-Y. Yun, and R. Balakrishnan, *Phys. Fluids,* **13**, 3061 (2001).

[22] S. Whitaker, *TiPM*, **1**, 3 (1986).

[23] R.E. Cunningham and R.J.J. Williams, *Diffusion in Gases and Porous Media*, Plenum Press, New York (1980).

[24] E. Skjetne and J.-L. Auriault, *TiPM*, **36**, 293 (1999).

[25] P.J.A.M. Kerkhof, *Chemical Eng. J.,* **64**, 319 (1996).

[26] P.J.A.M. Kerkhof and M.A.M. Geboers, *AlChE J.*, **51**, 79 (2005).

List of Figures

Figure 1: Modified diffusion bridge experimental apparatus; MFC: mass flow controller.

Figure 2: Top views of GDLs showing a decrease in pore size for increased PTFE loading and the difference between the PTFE for the Toray and SGL GDL. (a) Untreated Toray GDL; (b) 5 % PTFE Toray GDL; (c) 10 % PTFE Toray GDL; (d) GDL side of SGL 34 BC.

Figure 3: SEM images of GDL/MPLs with different PTFE loadings obtained by freeze fracturing. (a) 10 % PTFE Toray GDL/MPL; (b) 20 % PTFE Toray GDL/MPL.

Figure 4: Top views of the Toray and SGL MPL. (a) Toray MPL side showing the presence of GDL fibers which alter the structure of the MPL; (b) SGL 34 BC MPL side showing cracks which provide preferential paths for mass transport.

Figure 5: µCT images at slices into an SGL 34 BC. (a) 83 µm into the sample showing the GDL fibrous structure and PTFE distribution near the surface; (b) 167 µm into the sample highlighting MPL intrusion; (c) 283 µm into the sample showing the internal structure of the MPL including cracks and pores; (d) Image into the depth of the sample showing a non-uniform MPL distribution and pores in the MPL.

Figure 6: GDL pressure drop versus velocity results using nitrogen as the working gas.

Figure 7: GDL/MPL pressure drop versus velocity profiles using nitrogen as the working gas.

Figure 8: Comparison of experimental pressure drop versus velocity results using argon and oxygen gas to predicted profiles using Knudsen's expression and the compressible form of Darcy's law.

List of Tables

Table 1: Compressed thickness per layer and total compression of the GDLs and GDL/MPLs used in this study

Table 2: Comparison of the viscous permeability obtained for untreated Toray 090 GDL using nitrogen as the working gas with the literature. The difference is calculated relative to the nitrogen results obtained in this study

Table 3: Viscous permeability obtained for Toray GDLs with different PTFE loadings using nitrogen and helium gas and application of the compressible form of Darcy's law

Table 4: Viscous permeability values for GDL/MPLs with different PTFE loadings in the GDL obtained using the compressible form of Darcy's law

Table 5: Viscous permeability and effective pore diameter for GDL/MPLs with different PTFE loadings in the GDL obtained using Knudsen's expression

Table 6: Comparison of gas-dependent viscous permeability obtained using the compressible form of Darcy's law and gas-independent viscous permeability obtained using Knudsen's expression

Porous Material	GDL PTFE (%)	Thickness per layer (µm)	Compression (%)
SGL 34 BA	5	267 ± 5	6 ± 2
Toray 090 GDL	0	266 ± 15	5 ± 3
	5	262 ± 6	8 ± 1
	10	274 ± 0.7	8.0 ± 0.1
	20	270 ± 6	7 ± 1
	40	264 ± 14	5 ± 2
SGL 34 BC	5	303 ± 2	5.2 ± 0.2
Toray 090 GDL/MPL	5	263 ± 8	8 ± 1
	10	263 ± 11	6 ± 4
	20	255 ± 1	10.2 ± 0.9
	40	255 ± 4	7.9 ± 0.4

GDL Type		This work, N_2	This work, He	Gostick et al. [9]	Hussaini and Wang [12]
SGL 34 BA	B_v (10^{-12} m^2)	15.4	17.0	16.3	-
	Difference	-	+10.4 %	+5.84 %	-
Toray 0 % PTFE	B_v (10^{-12} m^2)	11.0	11.3	8.99	12.2
	Difference	-	+2.73 %	-18.3 %	+10.9 %

GDL Type	GDL PTFE (%)	$B_{v,\,N2}$ (10^{-12} m^2)	$B_{v,\,He}$ (10^{-12} m^2)	$B_{v,\,He}$ / $B_{v,\,N2}$ (10^{-12} m^2)
SGL 34 BA	5	15.4	17.0	1.10
Toray 090	0	11.0	11.3	1.03
	5	10.8	11.5	1.07
	10	9.02	9.64	1.07
	20	7.30	7.80	1.07
	40	2.72	3.35	1.23

GDL/MPL Type	GDL PTFE (%)	$B_{v, N2}$ (10^{-13} m^2)	$B_{v, He}$ (10^{-13} m^2)	$B_{v, He}$ / $B_{v, N2}$
SGL 34 BC	5	6.5 ± 0.2	7.7 ± 0.2	1.20 ± 0.05
Toray 090	5	3.9 ± 0.3	5.0 ± 0.3	1.3 ± 0.1
	10	4.1 ± 0.8	5.1 ± 0.9	1.2 ± 0.3
	20	1.4 ± 0.2	1.9 ± 0.2	1.3 ± 0.3
	40	0.5 ± 0.1	0.7 ± 0.2	1.5 ± 0.5

GDL/MPL Type	GDL PTFE (%)	B_v (10^{-13} m^2)	d_p^{eff} (µm)	$D_{O2}^{k,eff}$ (10^{-4} m^2 s^{-1})	$D_{N2}^{k,eff}$ (10^{-4} m^2 s^{-1})	$D_{H2}^{k,eff}$ (10^{-4} m^2 s^{-1})
SGL 34 BC	5	6.0 ± 0.2	2.07 ± 0.01	2.72 ± 0.01	2.91 ± 0.01	10.89 ± 0.05
Toray 090	5	3.3 ± 0.3	2.10 ± 0.02	2.77 ± 0.03	2.96 ± 0.03	11.1 ± 0.1
	10	3.6 ± 0.8	1.8 ± 0.2	2.4 ± 0.2	2.6 ± 0.2	9.7 ± 0.9
	20	1.1 ± 0.2	0.9 ± 0.1	1.2 ± 0.1	1.3 ± 0.2	4.9 ± 0.6
	40	0.4 ± 0.1	0.38 ± 0.08	0.5 ± 0.1	0.5 ± 0.1	2.0 ± 0.4

GDL/MPL Type	GDL PTFE (%)	$B_{v,\,N2}$ Darcy / B_v Kn	$B_{v,\,He}$ Darcy / B_v Kn
SGL 34 BC	5	1.096 ± 0.003	1.29 ± 0.02
Toray 090	5	1.18 ± 0.02	1.52 ± 0.06
	10	1.15 ± 0.02	1.43 ± 0.06
	20	1.23 ± 0.01	1.67 ± 0.02
	40	1.29 ± 0.05	1.9 ± 0.1

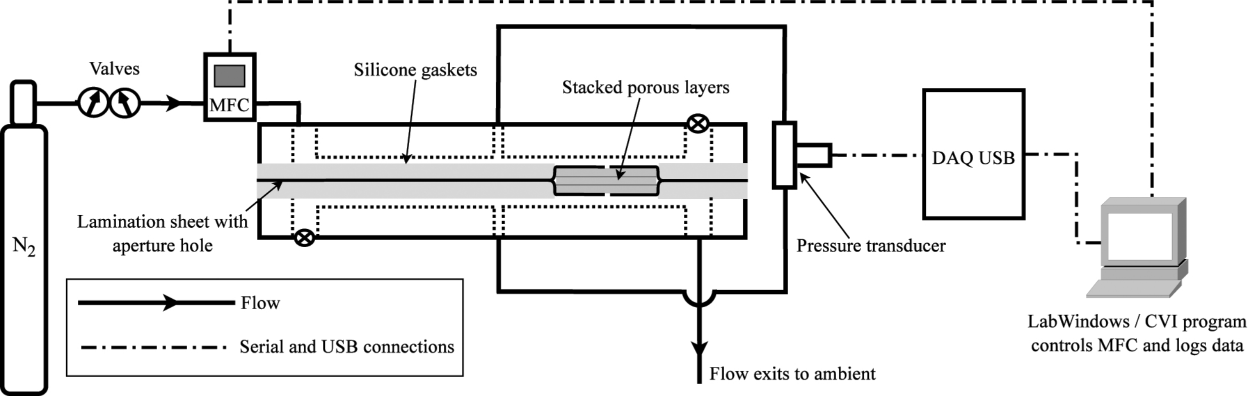
Valves
MFC
Silicone gaskets
Stacked porous layers
N_2
Lamination sheet with
aperture hole
DAQ USB
Pressure transducer
Flow
Serial and USB connections
Flow exits to ambient
LabWindows / CVI program
controls MFC and logs data

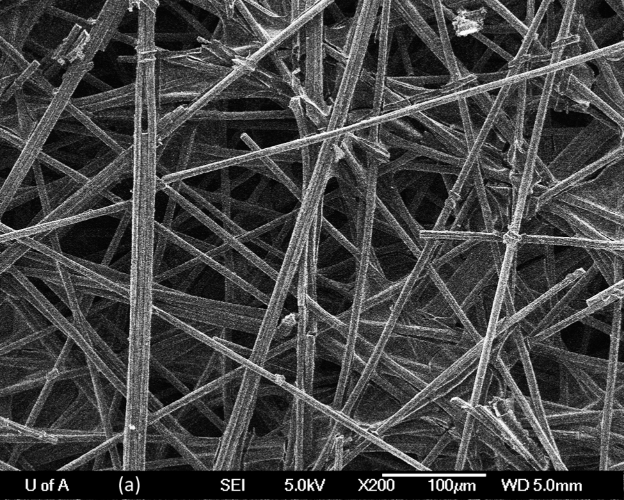
U of A
(a)
SEI
5.0kV
X200
100μm
WD 5.0mm

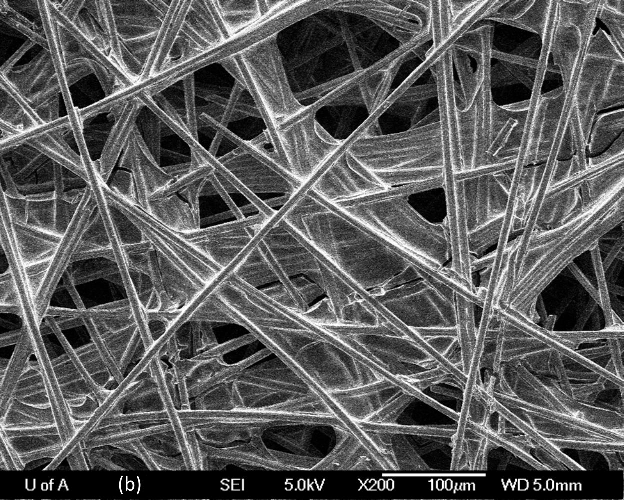
U of A
(b)
SEI
5.0kV
X200
100μm
WD 5.0mm

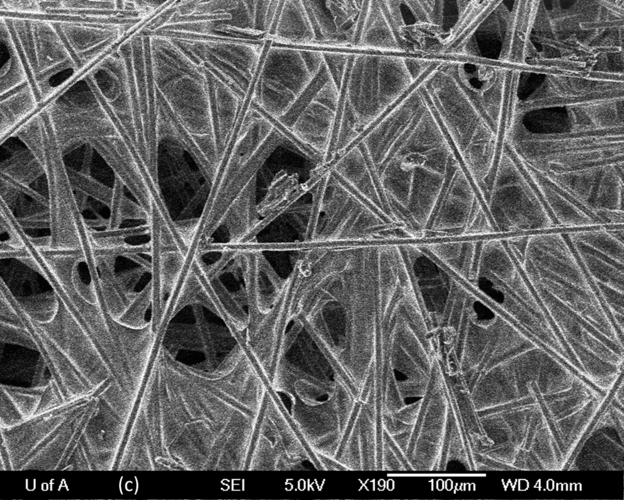
U of A
(c)
SEI
5.0kV
X190
100μm
WD 4.0mm

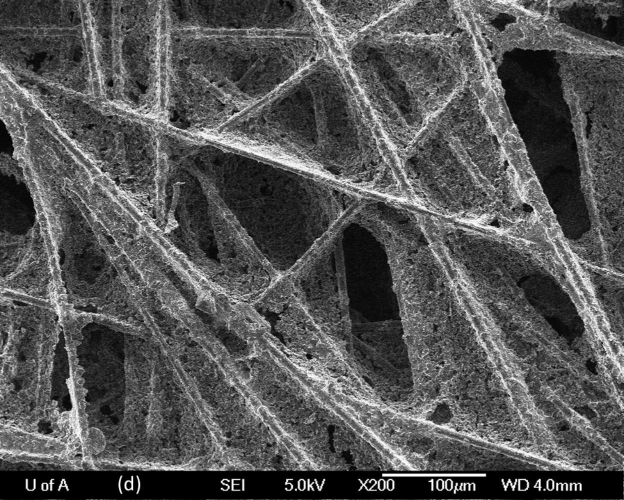
U of A
(d)
SEI
5.0kV
X200
100μm
WD 4.0mm

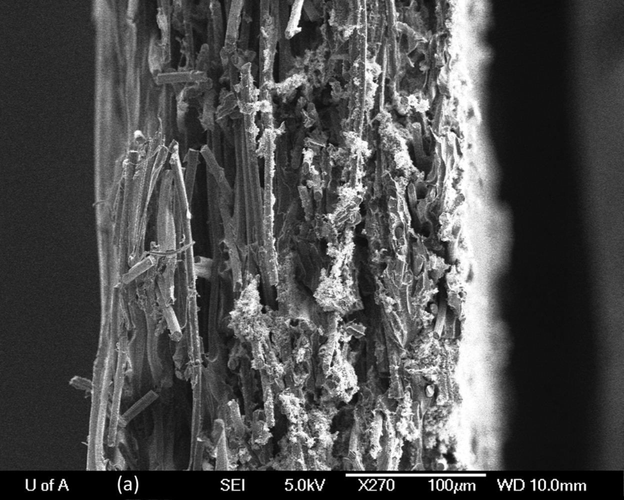
U of A
(a)
SEI
5.0kV
X270
100μm
WD 10.0mm

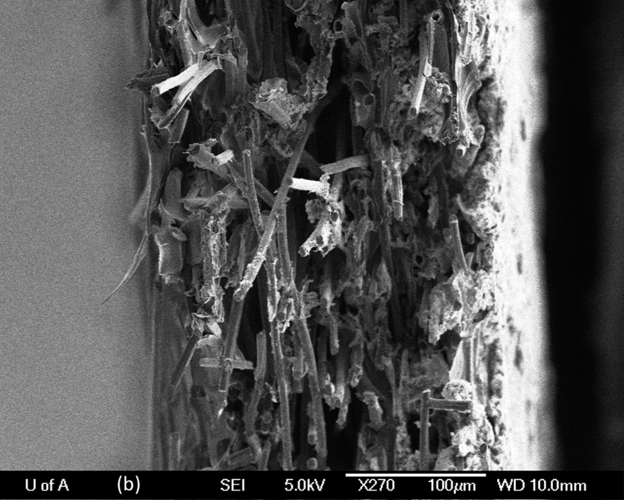

U of A
(b)
SEI
5.0kV
X270
100μm
WD 10.0mm

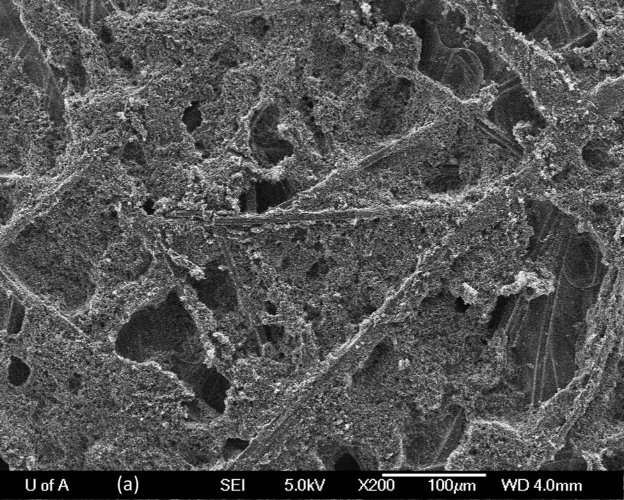
U of A
(a)
SEI
5.0kV
X200
100μm
WD 4.0mm

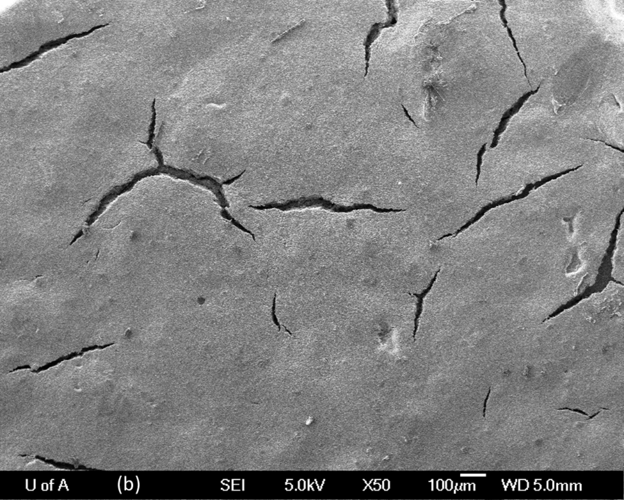
U of A
(b)
SEI
5.0kV
X50
100μm
WD 5.0mm

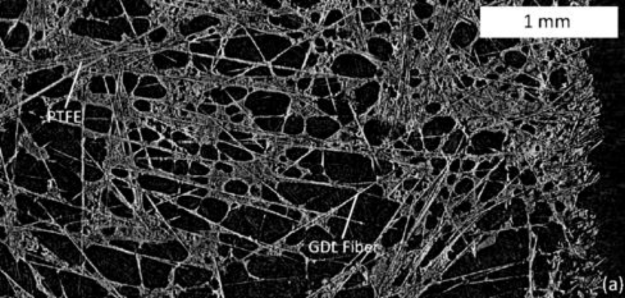
1 mm
PTFE
GDL Fiber
(a)

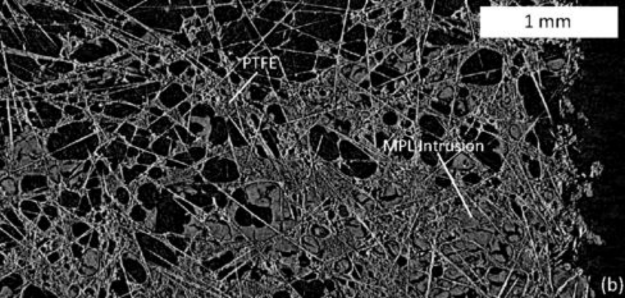
1 mm
PTFE
MPL Intrusion
(b)

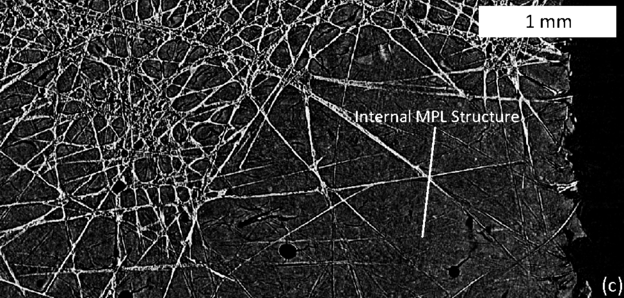
1 mm
Internal MPL Structure
(c)

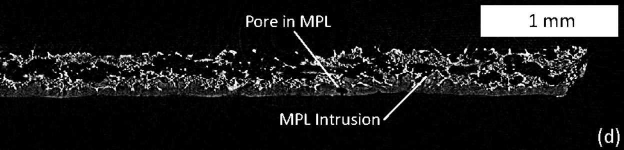
1 mm
Pore in MPL
MPL Intrusion
(d)

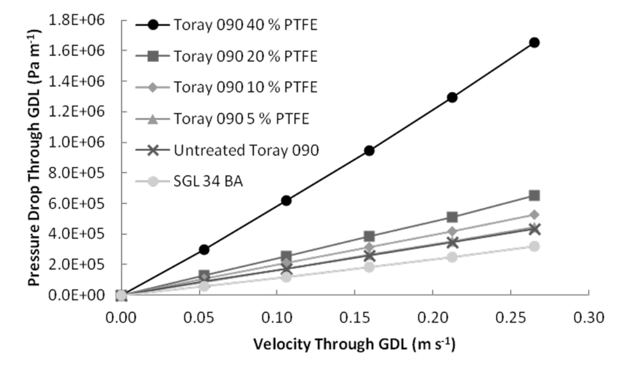

1.8E+06
1.6E+06
1.4E+06
1.2E+06
1.0E+06
8.0E+05
6.0E+05
4.0E+05
2.0E+05
0.0E+00
Pressure Drop Through GDL (Pa m-1)
0.00
0.05
0.10
0.15
0.20
0.25
0.30
Velocity Through GDL (m s-1)
Toray 090 40 % PTFE
Toray 090 20 % PTFE
Toray 090 10 % PTFE
Toray 090 5 % PTFE
Untreated Toray 090
SGL 34 BA

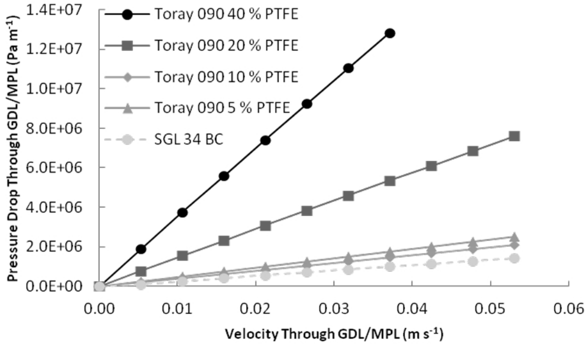

Toray 090 40 % PTFE
Toray 090 20 % PTFE
Toray 090 10 % PTFE
Toray 090 5 % PTFE
SGL 34 BC
Pressure Drop Through GDL/MPL (Pa m-1)
Velocity Through GDL/MPL (m s-1)
0.0E+00
2.0E+06
4.0E+06
6.0E+06
8.0E+06
1.0E+07
1.2E+07
1.4E+07
0.00
0.01
0.02
0.03
0.04
0.05
0.06

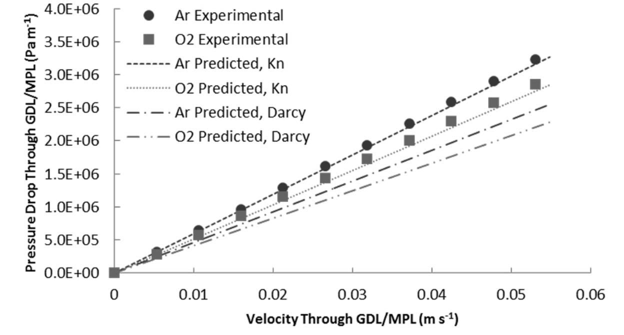
Ar Experimental
O2 Experimental
Ar Predicted, Kn
O2 Predicted, Kn
Ar Predicted, Darcy
O2 Predicted, Darcy
Pressure Drop Through GDL/MPL (Pa m-1)
Velocity Through GDL/MPL (m s-1)
0.0E+00
5.0E+05
1.0E+06
1.5E+06
2.0E+06
2.5E+06
3.0E+06
3.5E+06
4.0E+06
0
0.01
0.02
0.03
0.04
0.05
0.06